Combining Local PWV and Quantified Arterial Changes for Calibration-Free Cuffless Blood Pressure Estimation: A Clinical Validation

Cheng-Yan Guo, Chi-Hung Huang, Chia-Chi Chang, Kuan-Jen Wang, and Tung-Li Hsieh, *Member, IEEE*

***Abstract*—This study proposes a novel calibration-free cuffless blood pressure monitor (BPM). Unlike the cuffless BPM that requires timing correction with the traditional BPM, the calibration-free cuffless BPM can directly estimate the arterial blood pressure (BP) based on the hemodynamics mathematical model. Our proposed device integrates a pair of piezoelectric ceramics as pressure sensors to sense the pressure wave in the radial artery. It calculates the local pulse wave velocity (PWV) with our waveform detection algorithm of our proposed one. A photoplethysmogram (PPG) probe is set between the pair of pressure wave sensors. This PPG probe is used to monitor the radial artery's PPG intensity ratio (PIR). We design PPG signal processing algorithms to quantify the PIR. We recruited 129 participants for the BP monitoring experiment. Compared with the reference sphygmomanometer, the error mean ± standard deviations (STDs) systolic BP (SBP) was 2.1 ± 3.4, and the correlation r-value was 0.97. The diastolic BP (DBP) was 0.8 ± 4.2, the correlation r-value was 0.90, and $p < 0.05$ is taken as statistically significant. A new type of wearable continuous calibration-free BPM can replace the situation that requires the use of traditional ambulatory BPM and reduce patient discomfort. Our proposed BP measurement passed all ANSI/AAMI/ISO 81060-2:20181_5.2.4.1.2 data analysis criterion 1 and 2 standard requirements.**

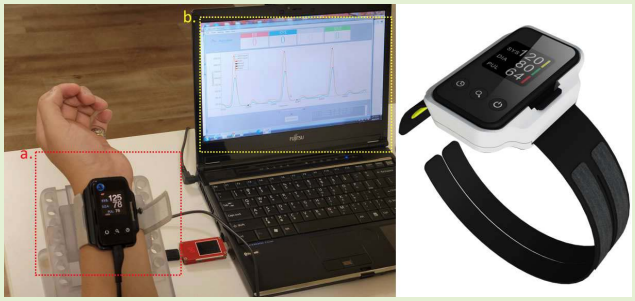

***Index Terms*— Blood pressure monitor (BPM), photoplethysmogram (PPG) intensity ratio, photoplethysmogram, pulse wave velocity (PWV), systolic blood pressure (SBP).**

I. Introduction

A CUFFLESS BPM is a BPM without an occluding cuff [1]. The difference between cuffless BPM and traditional BPM is that it does not need to pressurize the patient's arteries, reducing the discomfort caused by the procedure. Techniques used in this field include measuring physical parameters with electrocardiogram (ECG) and photoplethysmogram (PPG), phonocardiographic sensors, elastic modulus, dimensions, and stiffness of the intervening vessels, and establishing mathematical models to estimate blood pressure (BP) according to the sensor technology of choice. Ambulatory BP monitoring (ABPM) is the current gold standard for determining changes in an individual's BP and for determining hypertension [2]. Clinically, ABPM is valuable for controlling hypertension because it can better assess BP in patients with underlying hypertension affected by the white-coat effect [3]. However, patients wearing ABPM suffer from sleep disturbance as well as pain and skin irritation [4], [5]. Since cuffless BPM has no pressure cuff, it can greatly reduce the side effects and the interference of daily life and rest for patients using a traditional ABPM. Current cuffless BPMs [6] use ECG and PPG sensors to measure the pulse arrival time (PAT), convert it to pulse wave velocity (PWV), and then regress the measured PWV and the BP measured by the reference sphygmomanometer to get the correction coefficient [7]. However, studies have shown that PAT is affected by the pre-ejection period (PEP) [8], [9], meaning that PAT cannot accurately estimate PWV and, thus, BP. Moreover, in the current cuffless BPM correction procedure, the correction frequency needs to

Manuscript received 13 July 2022; revised 4 November 2022; accepted 13 November 2022. Date of publication 21 November 2022; date of current version 29 December 2022. The associate editor coordinating the review of this article and approving it for publication was Prof. Octavian Postolache. *(Cheng-Yan Guo and Tung-Li Hsieh are co-first authors.) (Corresponding author: Tung-Li Hsieh.)*

Cheng-Yan Guo and Kuan-Jen Wang are with Accurate Meditech Inc., New Taipei City 241406, Taiwan (e-mail: r04458006@ntu.edu.tw; stanley@accurate-meditech.com).

Chi-Hung Huang is with the Division of Cardiology, Department of Internal Medicine, Cathay General Hospital, Taipei 10630, Taiwan (e-mail: hchbox@cgh.org.tw).

Chia-Chi Chang is with Advanced Micro Devices Inc., Hsinchu 300052, Taiwan (e-mail: tammy.chang@amd.com).

Tung-Li Hsieh is with the Department of Electronic Engineering, National Kaohsiung University of Science and Technology, Sanmin, Kaohsiung City 807618, Taiwan (e-mail: tunglihsieh@gmail.com).

Digital Object Identifier 10.1109/JSEN.2022.3222588

be determined according to the technical details of different cuffless BPMs [10], and patients still cannot be exempted from the use of a traditional BPM. Even if the regression model is modified to a more complex machine learning model, using various physiological signal characteristics and demographics (e.g., age and sex) as parameters, and matching different hyperparameters to predict BP, it is unclear how much of the attained BP measurement accuracy, especially of the calibration-free device, is due to the actual hemodynamic measurement [11]. The Moens–Korteweg (MK) equation [12] in hemodynamics describes the relationship between PWV and BP, in which the arterial parameters must be considered. The characteristics of arterial hemodynamics differ between individuals, and only considering the correlation between PWV and BP would produce inaccurate BP measurements. To accurately estimate BP, calibration-free cuffless BPMs should not only be able to measure PWV accurately but also be able to monitor arterial distension. Since changes in arterial diameter (ΔD) correlate with pulse pressure (PP) [13], changes in arterial diameter can be quantified using the PPG intensity ratio (PIR) method. Therefore, this study proposes a calibration-free cuffless BPM measurement method using two piezoelectric sensors to measure the local PWV of the wrist radial artery combined with the physiological characteristics of arterial changes measured by the PPG probe. For this, we used a mathematical model based on hemodynamics to correlate PIR with arterial changes. This approach could integrate the sensor into a wearable device, affording more comfort to patients who require a traditional ABPM for long-term BP monitoring.

II. Our Contribution

We propose and implement a calibration-free cuffless BPM measurement method that uses a pair of piezoelectric sensors to measure the patient's pulse transit time (PTT) and convert it to local PWV. Also, we use a PPG sensor to detect the patient's PIR signals and quantify artery parameters using a hemodynamics-based mathematical model. Therefore, we have designed a wearable device that integrates these two sensors to achieve calibration-free cuffless BP monitoring. We verified it with ANSI/AAMI/ISO 81060-2, and our proposed BP measurement passed all ANSI/AAMI/ISO 81060-2:20181_5.2.4.1.2 data analysis criterion 1 and 2 standard requirements. This study provides patients with a solution to replace the traditional ABPM monitoring scenario, reducing patients' adverse reactions when BP is monitored for an extended period.

III. Calibration-Free Method of the Cuffless BPM

Our proposed method uses a pair of piezoelectric sensors and a PPG sensor set between them. These two types of sensors measure the pressure waveform and PIR of the patient's radial artery integrated with a PPG sensor, as shown in Fig. 1. The piezoelectric ceramic is rigid, and applying only a small deflection of the material is required to return a good signal. This makes the sensors very robust and tolerant of overpressure conditions and also means that they respond rapidly to changes in pressure [14]. Using a piezoelectric

Fig. 1. Piezoelectric sensor and PPG sensor are integrated.

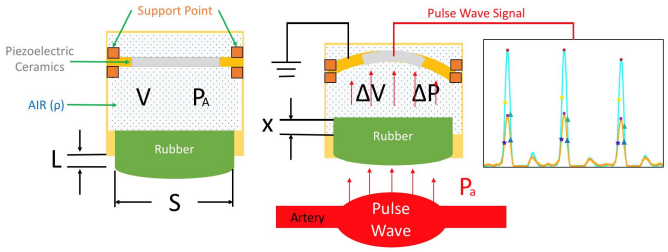

Fig. 2. Mechanical model of the piezoelectric sensor.

sensor, rather than a PPG sensor, to measure PWV avoids the need to consider the different characteristics of the PPG signal and the difference in PWV measured by the derivative method [15]. Therefore, PPG is used to measure the patient's PIR in this study and is related to arterial parameters and PP through a mathematical model. Setting the PPG probe between the two piezoelectric sensors ensures that when both piezoelectric sensors sense the pressure of the pulse wave, the PPG sensor is also above the radial artery and can receive the artery expansion signal.

A. Local PWV Measurement

In previous studies, we developed a piezoelectric sensor and algorithm [16] that can be used for PWV detection. Fig. 2 shows the mechanical model of the piezoelectric sensor. The volume change ΔV is generated when the pulse wave is transmitted via the induction period and skin motion. The internal pressure change ΔP of the sensor is the sum of the pressure before pressurization P_A and the pulse wave pressure P_a. The mass that pushes the rubber to compress the air when the artery expands is S $\times$ L multiplied by the air density. Note that the air density is not constant during the pulsed cycle. According to Newton's law, we can find the force of the piezoelectric ceramic. The piezoelectric signal generated by the piezoelectric ceramic is the pulse wave.

Fig. 3 shows the pulse wave sensor's analog front end (AFE). Our proposed device uses two pulse wave sensors and AFE. The output of the AFE is sampled by the 12-bit analog-to-digital converter (ADC) integrated into the microcontroller unit (MCU) of the ARM Cortex-M4 architecture. The sampling rate is 10 kHz, making the resolution of PTT in 0.1 ms. The parasitic capacitance of the piezoelectric ceramic is 8000 pF (at 120 Hz) [17]. The AFE can amplify the pulse wave signal, measured by the piezoelectric sensor, and filter it. Our filter design uses the second-order Sallen–Key architecture [18]. The cutoff frequencies of high-pass filters (HPFs) and low-pass filters (LPFs) are 0.58 and 10.6 Hz, respectively. The 12-bit ADC inside the MCU samples the pulse wave output

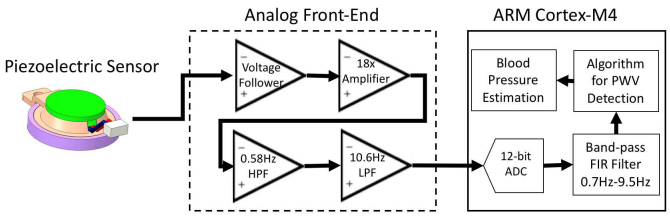

Fig. 3. Pulse wave sensor's AFE.

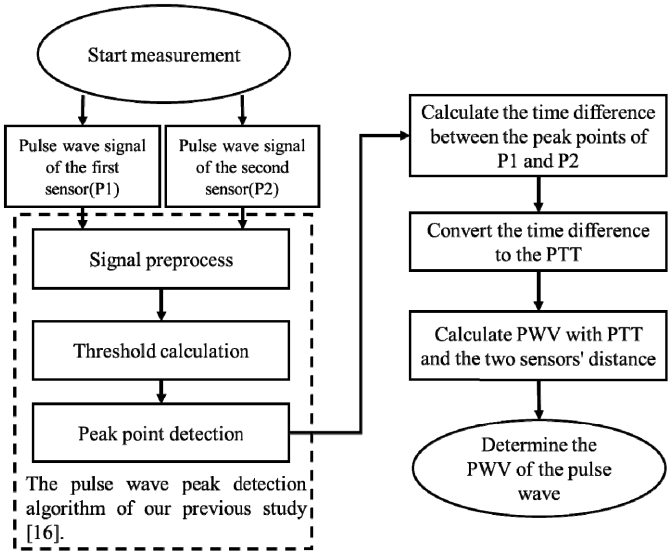

Fig. 4. Flowchart of the algorithm for determining PWV.

by the AFE at a sampling rate of 10 000 Hz. Through the finite impulse response (FIR) digital signal filtering algorithm running on the processor, the two-channel pulse wave sensor of the AFE output signal is filtered. Our design uses a bandpass filter of order 128 and uses the Kaiser window function, with the cutoff frequency set from 0.7 to 9.5 Hz [19], [20]. Based on the dynamic PWV detection algorithm developed in our past research, the PWV of the patient can be well detected. The algorithm can detect the feature points of the pulse wave and calculate the peak-to-peak value of the pulse wave signal at two different positions on the radial artery. As shown in the flowchart of Fig. 4, to determine the PWV between two pulse wave peaks, the time difference between the two pulse wave peaks at different positions needs to be converted to PTT after it can calculate PWV with PTT and two sensors' distance [21].

B. PPG Signal Process and PIR Estimate

When the pulse wave sensor detects the arterial pulse wave and can calculate the PWV, showing that the device is placed on the arterial segment of the human body, the PPG sensor is activated to sense the optical signal of arterial expansion. The PPG sensor is the MAX30101 integrated circuit produced by Analog Devices Inc. (ADI), which is a diffuse reflectance spectroscopy (DRS) sensor with three wavelengths of excitation light [22], [23]. The distance between the light-emitting diode (LED) and the photodiode (PD) is 3 mm. We set the ADC sampling rate of the PD to 100 Hz and the resolution to 18 bits. According to the Beer–Lambert law, the light path is arc-shaped. The photons start from the skin surface, penetrate deep into the tissue, before returning to the PD surface, and

Algorithm 1 I_H and I_L Detection Algorithm for PPG Signal

Inputs: PPG{index, value}, and gradient
is_I_H, is_I_L:= **FALSE**
if value > local_maxima **then**
local_maxima:= PPG{index, value}
end if
if value < local_minimal **then**
local_ minimal:= PPG{index, value}
end if
if is_emission == **TRUE** and x < local_maxima – gradient **then**
is_emission:= **FALSE,** is_I_H:= **TRUE**
falling:= PPG{index, value}
local_minimal:= local_maxima
result:= {is_ I_H, local_maxima}
end if
if is_emission == **FALSE** and x > local_minimal + gradient **then**
is_emission:= **TRUE,** is_ I_L:= **TRUE**
rising:= PPG{index, value}
local_maxima:= local_minimal
result:= {is_ I_L, local_minimal}
end if
if is_ I_H != **TRUE** and is_ I_L != **TRUE then**
result:= {-1, the current PPG signal is not a I_H or I_L }
end if
Outputs: result

are converted to an electron signal [24]. The path depth of photons in tissue depends on the wavelength of light. We chose infrared (IR) light with a wavelength of 880 nm as our PPG signal for estimating arterial changes. IR light can penetrate deeper into the tissue than visible wavelength light and can therefore obtain more tissue optical information [25].

Using PIR to estimate changes in arterial diameter is a feasible method [26]. However, it is necessary to filter the PPG signal to quantify the PIR of arterial changes accurately. Also, we would need to design a feature recognition algorithm based on dynamic thresholds to detect the minimal level and highest level of the ac signal of the PPG. To filter the PPG signal, we use the FIR filter algorithm. First, an HPF filters the PPG signal, which is then filtered a second time by an LPF. We set the cutoff frequency of low-pass filtering to 7.5 Hz and the cutoff frequency of high-pass filtering to 0.75 Hz.

The PPG signal after FIR filtering can use the feature detection algorithm, based on the dynamic threshold, to detect the minimal level I_L and highest level I_H of the PPG signal. We use the window size of half the sampling rate to calculate the dynamic threshold. When the window size is shorter, the response speed of the dynamic threshold is faster, and it is more sensitive to the change rate of the PPG signal. Equation (1) is the calculation method of the dynamic threshold, in which (2) is the formula of covariance (CV), which is used to calculate the previous rate of change of the signal intensity. Before calculating the CV, the average value of the signal needs to be determined by (3). The root mean square (rms) is the amplitude level of the signal, see (4). The gain can be adjusted manually according to the performance of different sensors, and the gain level of the dynamic threshold is set to 1 in this study.

The dynamic threshold of the current PPG signal is determined through (1). This threshold can be input into the

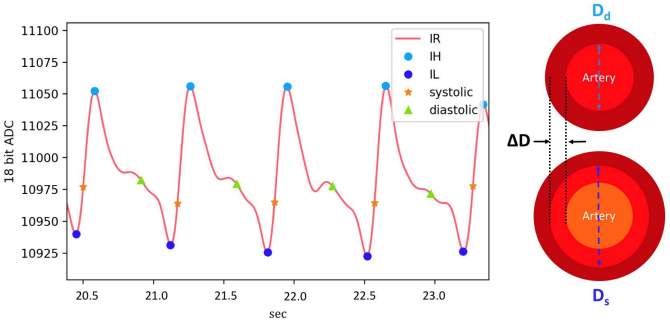

Fig. 5. PPG signals of different amplitudes according to the dynamic threshold, and the labeling of the feature points.

feature detection algorithm, which can dynamically identify the features in the PPG signal. The pseudocode of the feature detection algorithm proposed in this study is Algorithm 1 [27]. This algorithm can detect PPG signals of different amplitudes according to the dynamic threshold and label the feature points, as shown in Fig. 5, including the PPG signal's systole and diastole start points as well as the local maximum I_H and the local minimum I_L of the PPG signal. During the diastole phase, the arterial diameter is at its minimum level D_d, the absorption of light by the blood volume in the artery decreases, and the diffuse light intensity is at its highest level I_H. Conversely, during the systole phase, as the diameter of the artery increases to D_s, the absorption of light due to higher blood volume in the artery increases, causing diffuse light intensity to decrease to the minimum level I_L. ΔD is the change in arterial diameter from diastole to systole during cardiac cycles. It should be noted that the definition of the relationship between the PPG signal and the diameter of the artery must differ according to the design of the amplifier for the PD signal of the PPG sensor, specifically whether it is a noninverting amplifier or an inverting amplifier.

To make the IR light penetrate as deep as possible into the tissue and to improve the signal-to-noise ratio (SNR) of the PPG signal, when measuring arterial changes, the system will detect whether I_H is close to the saturation current 2^{18} measured by the ADC. When it is not close to the saturation current, the system will continue to increase the current of the LED constant current source for the PPG sensor until it reaches the required constant current source. Then, the last unsaturated current parameter will be used as the current setting of the LED constant current source for the PPG sensor

$$\text{gradient} = \text{RMS} \cdot \frac{\text{CV}}{100} \cdot \text{gain} \tag{1}$$

$$\text{CV} = \frac{\left(\sum_{k=0}^{N-1} x_k - \text{mean}\right)^2}{N} \tag{2}$$

$$\text{mean} = \frac{\sum_{k=0}^{N-1} x_k}{N} \tag{3}$$

$$\text{RMS} = \sqrt{\frac{\sum_{k=0}^{N-1} x_k^2}{N}}. \tag{4}$$

C. PIR-Arterial Change Estimation Based on Hemodynamic Model

The feature detection algorithm can accurately determine I_H and I_L of the PPG signal, and the PIR signal of the artery can be estimated. However, to build a correlation model of PIR-arterial diameter and PIR-PP, the arterial parameter ΔD and arterial PP should be considered as hemodynamic parameters, and the mathematical model must be based on hemodynamics.

In a study on the PPG analysis of arteries wrapped under tissue by the Monte Carlo simulation [28], arteries of different sizes had different rates of change for the PPG ac signal, and the amount of photons absorbed depended on blood volume. Blood volume is directly related to arterial size, so larger diameter arteries have higher absorption, which can be quantified and used to determine the arterial size, see (5), by normalizing the ac and dc signals of the PPG signal. The artery is under 1 cm of tissue. There is, therefore, an obvious relationship between the diameter of the artery and the normalized PPG signal. Furthermore, the blood vessel phantom experiment was used to verify that the variation of the artery and the arterial diameter was proportional to the rate of change of the signal, which was consistent with the results of the Monte Carlo simulation. However, in practice, the dynamic removal of the dc signal of the PPG signal is not easy [29], affecting the ratio of the normalized signal and causing a deviation. Therefore, a more accurate PIR method is used to normalize the PPG.

The relationship between arterial diameter change versus I_H and I_L can be expressed as (6) and (7) by the Beer–Lambert law [30]. The arterial expansion and blood volume changes produced by the cardiac cycle allow the DRS sensor to receive an ac signal. The dc signal is a tissue component, including the optical tissue information of the subject's epidermis, muscle, fat, and arterial tissue. $\alpha_{\text{DC}} = \varepsilon \times \text{c}$, where ε is the absorbance coefficient of human tissue and c is the material concentration of tissue and blood. d_{DC} is the dc component of the optical path of photons in human tissue, including the optical properties of refraction and reflection produced by different layers of tissue media. The product of the two contributes to the dc signal source of the tissue's diffuse reflectance spectrum. D_s and D_d are the systolic and diastolic states of the artery with the progression of the cardiac cycle, respectively. Through (8), I_H and I_L can be expressed as a function of the diffuse reflection light signal for arterial expansion, as the ratio of I_H to I_L is the PIR signal of the DRS sensor. Therefore, we can express the systole diameter D_s and the diastole diameter D_d as formula (9) [31], which means that the PIR changes with the artery diameter change of the cardiac cycle. α is a constant related to the optical absorption coefficients in the light path. The subject's arterial expansion volume can be estimated by modeling the correlation function between the normalized PIR signal and the arterial expansion volume ΔD

$$PPG_{\text{norm}} = \frac{\ln(\text{AC}_\lambda)}{\ln(\text{DC}_\lambda)} \tag{5}$$

$$I_L = I_0 \cdot e^{-\alpha_{\text{DC}} \cdot d_{\text{DC}}} \cdot e^{-\alpha \cdot D_s} \tag{6}$$

$$I_H = I_0 \cdot e^{-\alpha_{\text{DC}} \cdot d_{\text{DC}}} \cdot e^{-\alpha \cdot D_d} \tag{7}$$

$$\Delta D = D_s - D_d = \frac{\ln\left(\frac{I_H}{I_L}\right)}{\alpha} \tag{8}$$

$$\text{PIR} = \frac{I_H}{I_L} = e^{-\alpha \cdot \pi \cdot D \cdot (D_s - D_d)}. \tag{9}$$

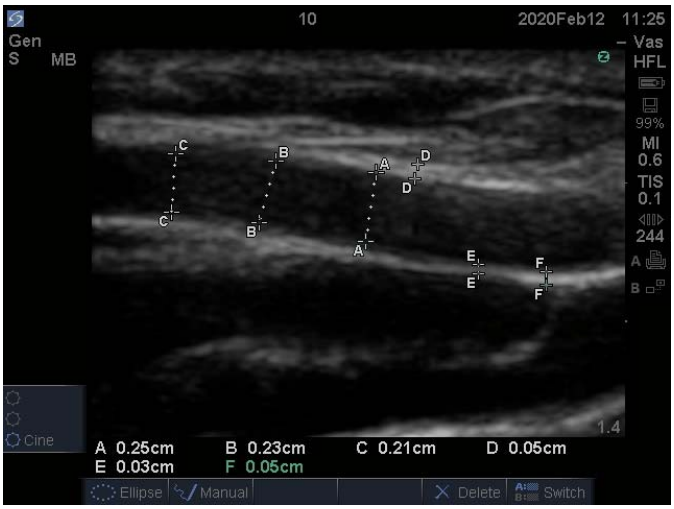

Fig. 6. Labels A, B, and C are artery diameters. Labels D, E, and F are IMT.

The normalized PIR signal was obtained and used to build a PIR-arterial diameter correlation model. We used an ultrasonic imaging device (M-turbo ultrasound system from Sonosite Inc.) to obtain the radial artery's diastolic diameter and record the normalized PIR signal for modeling the PIR-arterial diameter correlation model. In previous studies, the arterial diameter D and the instantaneous diastolic arterial diameter D_d differed by about 10% in each cardiac cycle, so it can be assumed that the two are approximately equivalent [32]. The MK equation of the hemodynamics model assumes an ideal circular and straight cylinder. Therefore, we selected different measurement points on the radial artery segment and averaged the artery diameter and wall thickness of the measurement points as the arterial parameters for building a correlation model to estimate the arterial expansion ΔD and arterial diameter D, as shown in Fig. 6. We used an ultrasound probe to measure and annotate the diameter and wall thickness of the radial artery [33]. We measured the ultrasound probe pressure-free on the surface between 2 and 6 cm above the styloid process [34] and referenced the method used to assess the radial artery in systemic disease to measure the arterial diameter and intima thickness [35] (the method for assessing the radial artery in systemic disease). Previous studies have shown that the arterial change rate is correlated with PP [36]. The PIR-PP correlation model of this study uses the difference between the values of systolic BP (SBP) and diastolic BP (DBP), measured by aneroid sphygmomanometer to reference PP, and is precomputed with the normalized PIR signal.

D. Calibration-Free Cuffless BP Measurement

During a cardiac cycle, the physiological changes of the radial artery can be described as a mathematical model composed of arterial dimensions, stiffness indices, and PTT. The model can quantify the elastic modulus of the artery and describe the compliance of the arterial segment. The hemodynamics theoretical model of the physiological characteristics can be extended and applied to cardiovascular system research [37]. The relationship between arterial pressure P and arterial diameter D can be expressed as (10), where P_d and D_d are the end-diastolic pressure and diameter, respectively, and β constant is the stiffness parameter usually related to the elasticity coefficient of human arteries. Equation (11) shows that the change of arterial pressure difference and arterial diameter are the primary variables that determine stiffness. Therefore, we can calculate the variation of the arterial diameter through the differential equation of the arterial pressure in (12), for the arterial diameter. Since the arterial diameter D and the instantaneous diastolic arterial diameter D_d differ by about 10% in each cardiac cycle, we can replace the arterial diameter term with the arterial cross-sectional area dA, as in (13), where the cross-sectional area A of the artery is calculated as $A = (\pi/4)\ D^2$ [38]. According to the Bramwell–Hill (BH) model [39], pressure pulses in the arteries produce local PWV. The local PWV can be expressed as intra-arterial pressure changes, and the PP is a function of the change in the arterial cross-sectional area, as in the modified BH model of (14), where ρ is the blood density. This study used the density of healthy human whole blood at 1.06 g/mL to calculate the parameter [40]. Equations (13) and (14) can be combined to obtain (15), which determines the value of the arterial local PWV in a cardiac cycle, dependent on the cross-sectional area gradient and the intra-arterial pressure level

$$\ln\left(\frac{P}{P_d}\right) = \beta\frac{D - D_d}{D - d} \tag{10}$$

$$\beta = \frac{\ln\left(\frac{P}{P_d}\right)}{\frac{D-D_d}{D_d}} \tag{11}$$

$$\frac{dP}{dD} = \frac{P\beta}{D_d} \tag{12}$$

$$\frac{dP}{dA} = \frac{2P\beta}{\pi D \cdot D_d} \tag{13}$$

$$\mathrm{PWV}^2 = \frac{A}{\rho}\frac{dP}{dA} \tag{14}$$

$$P = \frac{2 \cdot \rho \cdot \mathrm{PWV}^2 \cdot D_d}{\beta D}. \tag{15}$$

The BH model relates PWV to arterial compliance dA/dP, blood density ρ, and arterial cross-sectional area A, derived from the MK equation [41]. The MK equation is based on hemodynamics, such as with (16), (17), and (19). The MK equation describes the relationship between PWV and BP, where D is the diameter of the radial artery and h is the wall thickness of the radial artery, otherwise called intima-media thickness (IMT), ρ is the average density of whole blood, PTT is the pulse wave time difference measured by the relative distance L between the sensors, E is Young's modulus, P is the pressure, and E_0 and γ are coefficients with values of 1428.7 and 0.031, respectively [42]. Although E_0 and γ depend on the stiffness of the radial artery and vary between individuals [43], this study used mean values from previous clinical studies, assuming that E_0, γ, and ρ are constants, for validation. We combined (16) and (17) to obtain (18), where P in the MK equation approximates mean arterial pressure (MAP) [44]. So far, combining the PIR-arterial diameter correlation model and the PIR-PP correlation model, we can estimate the subject's MAP, PP, ΔD, and arterial diameter D.

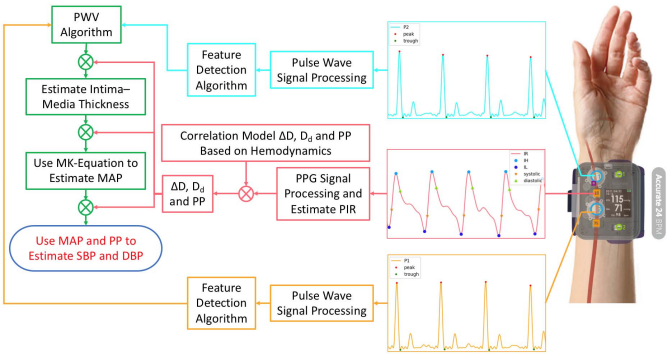

Fig. 7. Calculation flow of the calibration-free cuffless BPM.

Also, we can use the MK equation to enumerate the possible radial artery wall thickness h by assuming a reasonable range for MAP and using the recalculated MAP to track SBP and DBP with PP

$$\mathrm{PWV} = \sqrt{\frac{E_{\mathrm{inc}} \cdot h}{D \cdot \rho}} \tag{16}$$

$$E_{\mathrm{inc}} = E_0 \cdot \exp^{\xi \cdot P} \tag{17}$$

$$P = \frac{\ln\left(\frac{\mathrm{PWV}^2 \cdot \rho \cdot D}{h \cdot E_0}\right)}{\xi} \tag{18}$$

$$\mathrm{PWV} = \frac{L}{\mathrm{PTT}}. \tag{19}$$

Fig. 7 shows the calculation flow of the calibration-free cuffless BPM proposed in this study with the aforementioned theoretical model. First, the sensor detects the participant's pulse wave and PIR signal at the same time. The participant's local PWV can be calculated from the two pulse wave signals through our proposed algorithm, and the PIR can be measured using the DRS sensor. The normalized PIR signal is input into the prebuild PIR-arterial diameter and PIR-PP correlation models and a participant's estimated values of PP, ΔD, and D_d can be obtained. Since the wall thickness h of the participant's radial artery cannot be measured and estimated by the diffuse reflection light sensor, we refer to the known clinical research literature, assuming that the human MAP has a reasonable range under normal conditions [45]. Therefore, the MAP calculated by the MK equation has upper and lower bounds. Through the MK equation, the arterial wall thickness can be increased in 0.01 mm increments according to the arterial characteristics measured for different individuals. The possible range of the participant's arterial wall thickness can be enumerated, and the average value can be taken as the individual wall thickness parameter h. As shown in the enumeration algorithm of Algorithm 2, with h ranging from 0.01 to 1 mm in the MK equation calculation of MAP, if MAP exceeds the reasonable range, the value of the wall thickness must be unreasonable and vice versa. Therefore, the wall thickness value is considered reasonable if the MAP is within the reasonable MAP range. Since the MK equation is a nonlinear function, this enumeration can find a reasonable range of wall thickness according to the parameters of different individuals. This study chose to average this reasonable range as the individual radial artery wall thickness h. Finally, our

Algorithm 2 Use the MK Equation to Enumerate Arterial Wall Thickness's Upper and Lower Bounds

Inputs: PWV, Diameter, E_0, and ζ
wall_thickness:= 0.01
possible_thickness[0…n]
index:= 0
For wall_thickness < maximum_ wall_thickness
P:= **MK_Equaiton**(PWV, Diameter, E_0, ζ)
if P > MAP_Lower and P < MAP_Upper **then**
possible_thickness[index] = wall_thickness
index:= index + 1
end if
wall_thickness:= wall_thickness + 0.01
end for
result:= (possible_thickness[0] + possible_thickness[index - 1]) / 2
Outputs: result

proposed calibration-free cuffless BPM will extend the MAP and PP calculated by the MK equation to SBP and DBP with the formula of (20) [46]. The coefficient k in this study was set according to the clinical results and here is 0.76

$$\begin{cases} \mathrm{DBP} = \mathrm{MAP} - k \cdot \mathrm{PP} \\ \mathrm{SBP} = \mathrm{MAP} + (1-k) \cdot \mathrm{PP}. \end{cases} \tag{20}$$

IV. Clinical Study and Result

This study was approved by the Institutional Review Board (IRB) of the Cathay General Hospital, Taipei, Taiwan, and conducted according to the Declaration of Helsinki ethical principles for medical research on human participants. Each participant signed an informed consent form as defined by the IRB. The study protocol is retrospectively registered with the Taiwan Food and Drug Administration (IRB protocol number: CGH-P108003). In the clinical analysis in this section, our proposed calibration-free cuffless BPM is called Accurate24 BPM, and the sphygmomanometer for reference is called SM. The participants were equipped with Accurate24 BPM on the left wrist, sitting position with the wrist at heart level to remove hydrostatic pressure differences. A sphygmomanometer cuff of appropriate size was positioned on the participant's left upper arm at heart level. Study participants were comfortably seated with their backs and arms supported.

A. Study Protocol and Population

This comparative study followed ANSI/AAMI/ISO 81060-2:20181 [47]. Male and female volunteers totaling 129 subjects were included. The algorithm passed Criterion 2. The distribution of SBP and DBP is shown in Fig. 8(a) and (b), respectively.

BP measurements were taken by trained observers in stations. The clinical study method stated that observers shall be trained in using the proper methodology for performing a resting BP reading with the SM (reference reading) and an Accurate24 BPM device reading (subject under test) lasting at least 60 s, interchanging the reference and subject devices, with three replications of the process.

All data from a subject were excluded if the following conditions hold.

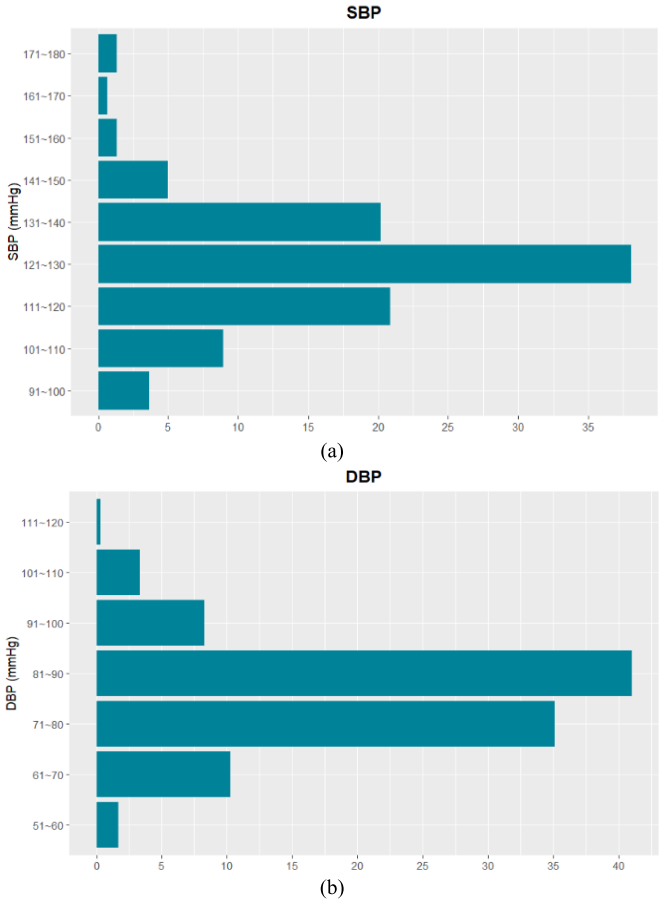

Fig. 8. Distribution of (a) SBP and (b) DBP.

1) Any two reference SBP values differed by more than 12 mmHg (160 kPa).

2) Any two reference DBP values differed by more than 8 mmHg (107 kPa).

B. Statistical Analysis

In this study, two measurement methods were compared: the novel method in this study (the Accurate24 BPM device) and an established one (a standard Korotkoff manometry device). We aimed to determine whether these two methods could be used interchangeably and whether our novel method could replace the established one.

In this study, the collected data for BP measurements were analyzed for mean, maximum, minimum, median, standard deviation (STD), and confidence values (Tables I and II). If the novel measurement technique agreed sufficiently with the established technique, it would be possible to replace it. Agreement between these techniques was analyzed using the Bland–Altman method, which calculates the mean difference between two methods of measurement (the "bias") and looks at the 95% limit of agreement of the mean difference 2STD. It is expected that the 95% limit includes 95% of differences between the two measurement methods. The presentation of the 95% limits of agreement allows for visual judgment of how well two methods of measurement agree. The smaller the range between these two limits, the better the agreement. Linear correlation is a measure of dependence or association between two random variables. The correlation provides a measure of the degree to which these two variables tend to "move together." The Pearson correlation coefficient is bounded between -1 and 1 making it easy to understand the intensity of the linear dependence between two random variables. The closer the correlation coefficient is to 1, the greater the positive linear dependence between the variables, and the closer it is to -1, the greater the negative linear dependence between them. When the correlation equals zero, the variables do not display any of these two tendencies. The Accurate24 BPM device application was compared to a standard Korotkoff manometry device and the differences between their readings were analyzed as explained in the following.

TABLE I
DEMOGRAPHIC AND CLINICAL CHARACTERISTICS OF THE STUDY PARTICIPANTS

Characteristic	Pass requirements
Subject, n	129
Age, n (%)	
≤ 30 years	18 (14.0)
31-40 years	16 (12.4)
41-50 years	60 (46.5)
51-60 years	23 (17.8)
> 60 years	12 (9.3)
Sex, n (%)	
Male	89 (69.0)
Female	40 (31.0)
Recruitment BP (mmHg)	
SBP	
Mean ± SD	125.5±13.0
Median (Range)	125.7 (92,175)
DBP	
Mean ± SD	80.7±8.7
Median (Range)	81 (59,109)

TABLE II
OBSERVER MEASUREMENT IN EACH RECRUITMENT RANGE

SBP (mmHg)		DBP (mmHg)	
BP pairs, n	302	BP pairs, n	302
Overall		Overall	
Mean ± SD	125.1±13.2	Mean ± SD	80.8±9.4
Median (Range)	125 (92,178)	Median (Range)	81 (55,111)
Low (<130), n (%)	207 (68.5)	Low (<80), n (%)	132 (43.7)
Medium (130-160), n (%)	89 (29.5)	Medium (80-100), n (%)	157 (52.0)
High (>160), n (%)	6 (2.0)	High (>100), n (%)	13 (4.3)
Differences (Ref: SM)		Differences (Ref: SM)	
Mean ± SD	2.1±3.4	Mean ± SD	0.8±4.2
Median (Range)	3 (-10,12)	Median (Range)	2 (-12,10)

C. Result

One hundred twenty-nine subjects had valid data sets and were included in the analyses, of which there were 40 females and 89 males. The Pearson correlation and Bland–Altman

TABLE III
PEARSON CORRELATION AND BLAND–ALTMAN ANALYSIS

	SBP (mmHg)	DBP (mmHg)
Correlation (ref: SM)		
R^2	0.94	0.81
R	0.97*	0.90*
Bland-Altman analysis		
Requirements, (Means±2SD)	(-4.51,8.81)	(-7.43,8.94)
Achieved, n (%)	281 (93.05)	280 (92.72)

*P *value* ≤ 0.05.

TABLE IV
VALIDATION STUDY RESULTS

	Pass requirements	Achieved	
		SBP	DBP
Criterion 1			
BP pairs:302			
Means (*mmHg*)	≤ 5	2.15	0.75
SD (*mmHg*)	≤ 8	3.40	4.18
Results		**pass**	**pass**
Criterion 2			
Subject:129			
SD (*mmHg*)	≤ 6.58/6.89	3.21	3.97
Results		**pass**	**pass**
Results		**pass**	

ANSI/AAMI/ISO 81060-2:2018_5.2.4.1.2 Data analysis Criterion 1 & 2

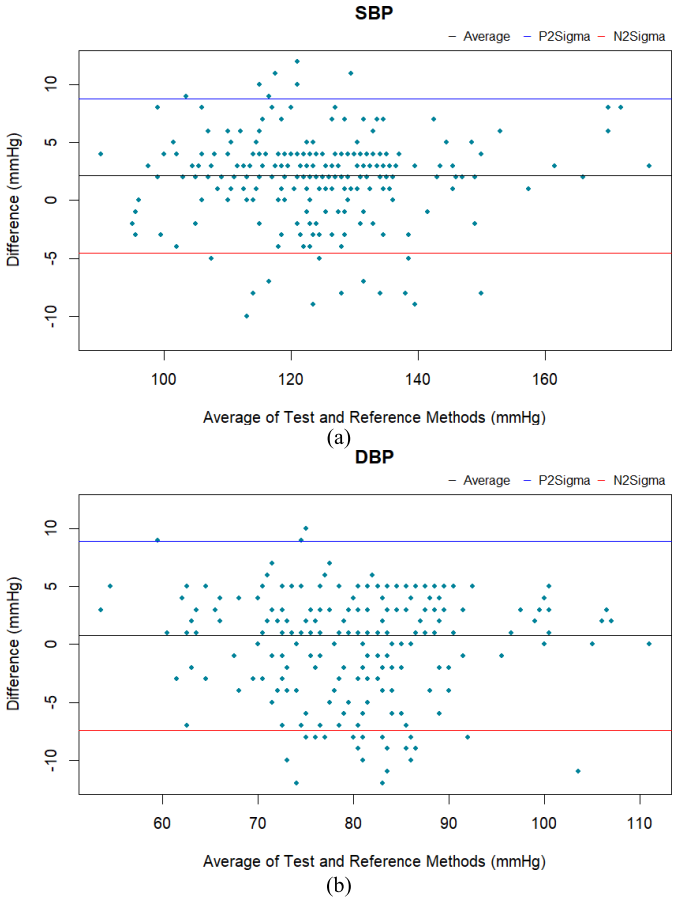

Fig. 9. Bland–Altman plot for (a) SBP and (b) DBP.

analysis between Accurate24 BPM and SM are shown in Table III.

For the SBP analysis, we found that $R^2 = 0.94$, which means that $R = 0.97$, showing that 97% of the data sets are, or are very close to, equal. For the DBP analysis, we found that $R^2 = 0.81$, which means that $R = 0.90$, showing that 90% of the data sets are, or are very close to, equal.

The Mean and SD of the validation study results of criterions 1 and 2 between the reference SM and subject device readings are shown in Table IV.

The ANSI/AAMI/ISO 81060-2:2018 Standard Criterion 1 requires a mean ±SD difference of ≤5 ± 8 mmHg. The Midmark algorithm clearly passed this criterion. Criterion 2 requires a smaller SD value, using a sliding scale depending on the mean SBP and DBP differences. For SBP, the mean value of 2.15 mmHg gives an upper limit for SD of 6.58, and for the DBP difference of 0.75, the upper limit for SD is 6.89. The algorithm passed criterion 2. The required Bland–Altman plots of SBP and DBP are shown in Fig. 9(a) and (b), respectively.

The Accurate24 BPM device was compared to the gold standard SM device by plotting a visual chart expressing the correlation between their readings in Fig. 10(a) and (b).

Another protocol, from the European Hypertension Society, expresses the data distribution as the percent of readings within 5, 10, and 15 mmHg in comparison to the reference BP values. While the Accurate24 BPM device recorded all values, manometry values were taken periodically as detailed earlier. Thus, we compared the manometer values to the Accurate24 BPM device values recorded at the same time. For Accurate24 BPM measurements according to the international protocol (revision 2010) [48], data are shown in Table V and Fig. 11.

D. Discussion

The data demonstrated that the Accurate24 Noninvasive BP monitor (BPM) for BP measurement passed all ANSI/AAMI/ISO 81060-2:20181_5.2.4.1.2 data analysis criterion 1 and 2 standard requirements. The Accurate24 Noninvasive BPM also surpassed requirements for the European Hypertension Society protocol data analysis for both SBP and DBP. These tests in adults show that the Accurate 24 BPM sensors and applications achieved the required range and were defined as having acceptable error levels by the European international protocol for BP devices, as shown in Table V. For accuracy in ≤5 mmHg, the proportion of Accurate24 BPM in SBP and DBP is 86.8% and 85.8%, respectively, both of which meet the European international protocol (73%). For accuracy in ≤10 mmHg, the proportion of Accurate24 BPM in SBP and DBP is 99.0% and 98.7%, respectively, both of which meet the European international protocol (87%). For accuracy in ≤15 mmHg, the proportion of Accurate24 BPM in SBP and DBP is 100% and 100%, respectively, both of which meet the European international protocol (96%).

V. LIMITATIONS AND FUTURE WORKS

Although the calibration-free cuffless BPM proposed in this study passed the clinical gold standard, according to the

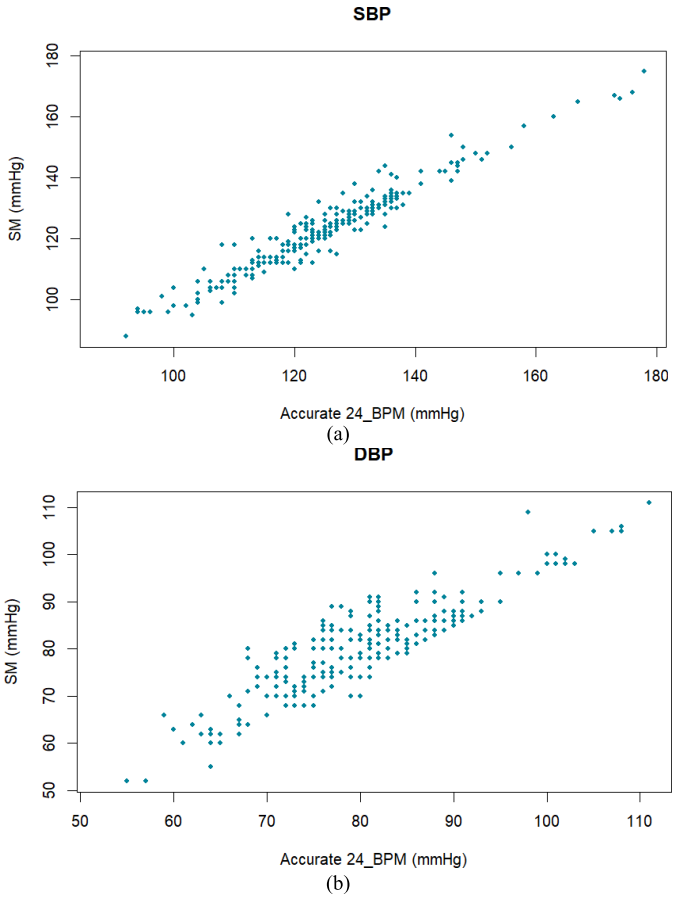

Fig. 10. Scatter plot between Accurate_24 BPM and SM. (a) SBP. (b) DBP.

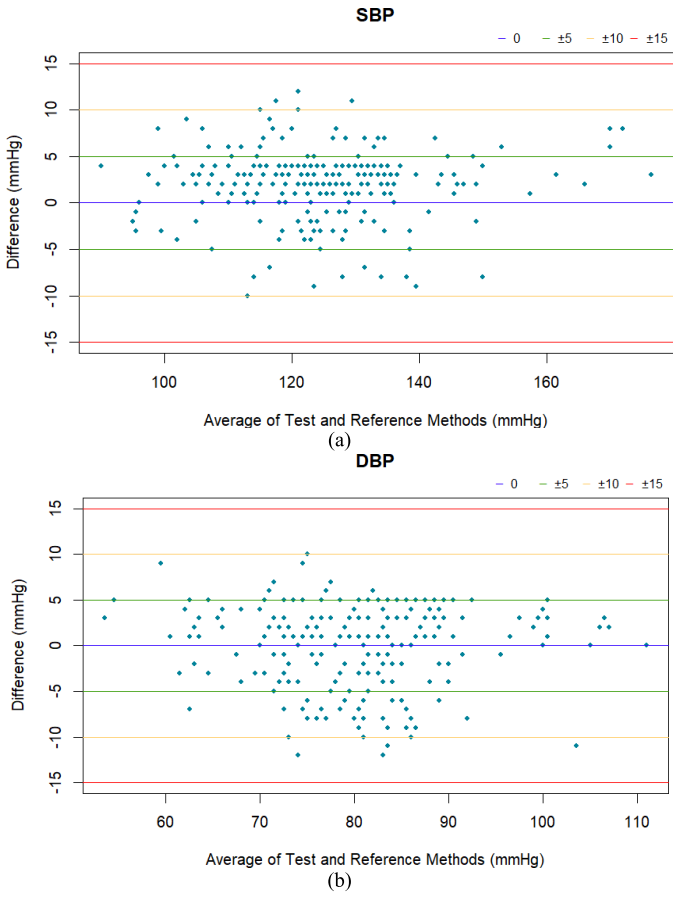

Fig. 11. Accurate24 BPM measurements in relation to the ESH international protocol (revision 2010). (a) SBP. (b) DBP.

TABLE V
VALIDATION STUDY RESULTS RELATING TO THE EHS PROTOCOL IN PERCENTAGE OF DIFFERENCE

Difference	≤ 5 mmHg	≤ 10 mmHg	≤ 15 mmHg
Required %	73.7%	87.9%	97.0%
Accurate24 BPM			
SBP, n (%)	262 (86.8)	299 (99.0)	302 (100.0)
DBP, n (%)	259 (85.8)	298 (98.7)	302 (100.0)

results, our proposed method still has two points to improve. First, according to the relationship described by the MK equation, the PWV primarily contributes to the result of the MAP calculation. The measurement of the local PWV of the arterial segment is performed over a short distance, resulting in small PTT measurement errors being amplified when converted to local PWV. Therefore, improving the measurement performance of the sensor, such as by increasing the sampling rate and resolution, can effectively reduce the STD value in the clinical results and increasing measurement precision. The application scenarios of beat-to-beat BP estimation will be possible in the future. Second, further research is required for calculating Young's modulus in the MK equation. This coefficient makes the relationship between MAP and PWV nonlinear. Although we calculate the coefficient with data obtained from previous clinical experiments, there are differences in arterial stiffness between individuals in practical applications, which leads to bias in the results of BP estimation. Therefore, finding a feasible technical means to measure the arterial stiffness of subjects noninvasively, and to calculate the nonlinear function of the arterial stiffness for each subject, would reduce the overall BP estimation bias. Normal subjects' arterial blood contains dyshemoglobin, which is a hemoglobin derivative. The two dyshemoglobins that affect tissue oxygenation are methemoglobin (MetHb) and carboxyhemoglobin (COHb), which are usually present in low concentrations in normal subjects in the blood [49]. The main substances that absorb IR light in the blood are oxyhemoglobin and hemoglobin. The absorption ratio of MetHb and COHb is low. However, when the subject is carbon monoxide poisoning or exposed to some chemical, it may increase MetHb and COHb [50]. In this study, using single-wavelength quantitative technology may cause errors, so multiwavelength quantitative technology is a future research direction that can quantify more substances to reduce inaccurate factors.

VI. CONCLUSION

This study proposes a new calibration-free cuffless BPM technique, which uses a pair of high-sensitivity piezoelectric sensors to measure the local PWV, and a DRS sensor to quantify the PIR signal, of the radial artery. With this, we used principles based on hemodynamics and tissue optics to estimate BP. Our proposed calibration-free cuffless BPM has been clinically validated, showing that the technology passed all ANSI/AAMI/ISO 81060-2:20181_5.2.4.1.2 data analysis

criterion 1 and 2 standard requirements. In the trend of popularization of home medical care in the future, we believe that the sensing technology in this study can be integrated into wearable devices, with measurements based on hemodynamics, making it possible to provide beat-to-beat BP monitoring. This advantage could enable future research on hypertension to shorten the monitoring period from every hour to every minute. The improved performance of BP monitoring technology provides a powerful new tool for research in hypertension.

Acknowledgment

Cheng-Yan Guo, Chi-Hung Huang, Chia-Chi Chang, Tung-Li Hsieh, and Kuan-Jen Wang conceived the presented idea. Chia-Chi Chang and Cheng-Yan Guo developed the theory and performed the computations. Chia-Chi Chang, Tung-Li Hsieh, and Cheng-Yan Guo verified the analytical methods. Chi-Hung Huang and Kuan-Jen Wang encouraged the investigation (a specific aspect) and supervised the findings of this work. All authors discussed the results and contributed to the final manuscript.

References

[1] *IEEE Standard for Wearable Cuffless Blood Pressure Measuring Devices*, Standard 1708–2014, IEEE Xplore, I. S. Association, 2014.

[2] T. G. Pickering, D. Shimbo, and D. Haas, "Ambulatory blood-pressure monitoring," *New England J. Med.*, vol. 354, no. 22, pp. 2368–2374, Jun. 2006.

[3] A. J. Viera, K. Lingley, and A. L. Hinderliter, "Tolerability of the oscar 2 ambulatory blood pressure monitor among research participants: A cross-sectional repeated measures study," *BMC Med. Res. Methodol.*, vol. 11, no. 1, p. 59, Dec. 2011.

[4] M. S. van der Steen, J. W. M. Lenders, and T. Thien, "Side effects of ambulatory blood pressure monitoring," *Blood Pressure Monitor.*, vol. 10, no. 3, pp. 151–155, Jun. 2005.

[5] L. Elliot and P. Iqbal, "Factors associated with probability of patient rejecting a repeat 24 h ambulatory blood pressure monitoring, despite recommendation by the physician," *Blood Pressure Monit.*, vol. 8, no. 5, pp. 191–194, 2003.

[6] G. Zhang, S. A. McCombie, R. Greenstein, and D. B. McCombie, "Assessing the challenges of a pulse wave velocity based blood pressure measurement in surgical patients," in *Proc. Annu. Int. Conf. IEEE Eng. Med. Biol. Soc.*, Aug. 2014, pp. 574–577.

[7] A. Steptoe, H. Smulyan, and B. Gribbin, "Pulse wave velocity and blood pressure change: Calibration and applications," *Psychophysiology*, vol. 13, no. 5, pp. 488–493, 1976.

[8] J. Muehlsteff, X. L. Aubert, and M. Schuett, "Cuffless estimation of systolic blood pressure for short effort bicycle tests: The prominent role of the pre-ejection period," in *Proc. Int. Conf. IEEE Eng. Med. Biol. Soc.*, Aug. 2006, pp. 5088–5092.

[9] S. L.-O. Martin et al., "Weighing scale-based pulse transit time is a superior marker of blood pressure than conventional pulse arrival time," *Sci. Rep.*, vol. 6, no. 1, pp. 1–8, 2016.

[10] D. B. McCombie, P. A. Shaltis, A. T. Reisner, and H. H. Asada, "Adaptive hydrostatic blood pressure calibration: Development of a wearable, autonomous pulse wave velocity blood pressure monitor," in *Proc. 29th Annu. Int. Conf. IEEE Eng. Med. Biol. Soc.*, Aug. 2007, pp. 370–373.

[11] R. Mukkamala et al., "Evaluation of the accuracy of cuffless blood pressure measurement devices: Challenges and proposals," *Hypertension*, vol. 78, no. 5, pp. 1161–1167, 2021.

[12] Y. Ma, J. Choi, A. Hourlier-Fargette, Y. Xue, H. U. Chung, and J. Y. Lee, "Relation between blood pressure and pulse wave velocity for human arteries," *Proc. Nat. Acad. Sci. USA*, vol. 115, no. 44, pp. 11144–11149, 2018.

[13] X.-R. Ding, Y.-T. Zhang, J. Liu, W.-X. Dai, and H. K. Tsang, "Continuous cuffless blood pressure estimation using pulse transit time and photoplethysmogram intensity ratio," *IEEE Trans. Biomed. Eng.*, vol. 63, no. 5, pp. 964–972, May 2016.

[14] M. S. Vijaya, *Piezoelectric Materials and Devices: Applications in Engineering and Medical Sciences*. London, U.K.: CRC Press, 2017.

[15] J. Runciman, M. McGregor, G. Silva, G. Monteith, L. Viel, and L. G. Arroyo, "A new statistical phase offset technique for the calculation of in vivo pulse wave velocity," *Artery Res.*, vol. 13, p. 17, Mar. 2016.

[16] C.-Y. Guo, K.-J. Wang, and T.-L. Hsieh, "Piezoelectric sensor for the monitoring of arterial pulse wave: Detection of arrhythmia occurring in PAC/PVC patients," *Sensors*, vol. 21, no. 20, p. 6915, Oct. 2021.

[17] E. Bartolome, "Signal conditioning for piezoelectric sensors," Texas Instrum., Dallas, TX, USA, Appl. Rep. SLOA033A, Oct. 2010, p. 10.

[18] J. Karki, "Analysis of the Sallen-Key architecture," Texas Instrum., Dallas, TX, USA, Appl. Rep. SLOA024B, Tech. Rep., 2002.

[19] Y. Lim and S. Parker, "FIR filter design over a discrete powers-of-two coefficient space," *IEEE Trans. Acoust., Speech, Signal Process.*, vol. ASSP-31, no. 3, pp. 583–591, Jun. 1983.

[20] G. Jinding, H. Yubao, and S. Long, "Design and FPGA implementation of linear FIR low-pass filter based on Kaiser window function," in *Proc. 4th Int. Conf. Intell. Comput. Technol. Autom.*, Mar. 2011, pp. 496–498.

[21] P. L. M. Kerkhof and V. M. Miller, *Sex-specific Analysis of Cardiovascular Function*, 1st ed. Cham, Switzerland: Springer, 2018.

[22] (2021). *Maximintegrated*. [Online]. Available: https://www.maximintegrated.com/en/products/interface/signal-integrity/MAX30101.html

[23] P. C. Schönle, "*A Power Efficient Spectrophotometry & PPG Integrated Circuit for Mobile Medical Instruments*, 2017th ed. Konstanz, Germany: Hartung-Gorre, 2017.

[24] V. O. Rybynok and P. A. Kyriacou, "Beer-lambert law along non-linear mean light pathways for the rational analysis of photoplethysmography," *J. Phys., Conf.*, vol. 238, Jul. 2010, Art. no. 012061.

[25] Y.-H. Kao, P. C.-P. Chao, Y. Hung, and C.-L. Wey, "A new reflective PPG LED-PD sensor module for cuffless blood pressure measurement at wrist artery," in *Proc. IEEE SENSORS*, Oct. 2017, pp. 1–3.

[26] Y. Chen, Y. Zhu, H. T. Ma, and H. Huang, "A study of photoplethysmography intensity ratio in hypertension," in *Proc. IEEE Int. Conf. Real-time Comput. Robot. (RCAR)*, Jun. 2016, pp. 317–320.

[27] P. Spachos, J. Gao, and D. Hatzinakos, "Feasibility study of photoplethysmographic signals for biometric identification," in *Proc. 17th Int. Conf. Digit. Signal Process. (DSP)*, Jul. 2011, pp. 1–5.

[28] A. Chaturvedi, S. A. Shukair, M. Vijayvergia, P. Le Rolland, J. W. Gunn, and H. Subramanian, "Intraoperative blood vessel detection and quantification: A Monte Carlo study," *J. Biomed. Opt.*, vol. 23, no. 6, pp. 1–9, 2018.

[29] D. Pollreisz and N. TaheriNejad, "Detection and removal of motion artifacts in PPG signals," *Mobile Netw. Appl.*, vol. 27, no. 2, pp. 728–738, Apr. 2019.

[30] X.-R. Ding and Y.-T. Zhang, "Photoplethysmogram intensity ratio: A potential indicator for improving the accuracy of PTT-based cuffless blood pressure estimation," in *Proc. 37th Annu. Int. Conf. IEEE Eng. Med. Biol. Soc. (EMBC)*, Aug. 2015, pp. 398–401.

[31] X. Ding, B. P. Yan, Y.-T. Zhang, J. Liu, N. Zhao, and H. K. Tsang, "Pulse transit time based continuous cuffless blood pressure estimation: A new extension and a comprehensive evaluation," *Sci. Rep.*, vol. 7, no. 1, p. 11554, 2017.

[32] O. Vriz et al., "Comparison of sequentially measured Aloka echo-tracking one-point pulse wave velocity with SphygmoCor carotid–femoral pulse wave velocity," *SAGE Open Med.*, vol. 1, Oct. 2013, Art. no. 2050312113507563.

[33] J. C. Carretero, F. C. Montoya, M. G. Barez, M. C. Montoya, M. O. Hernández, and R. Larrainzar-Garijo, "Description and analysis of the dynamic and morphological flow pattern of the main arteries of the wrist and hand in a healthy Spanish population," *Rev. Esp. Cir. Ortop. Traumatol.*, vol. 64, no. 3, pp. 167–176, 2020.

[34] Z. Domagała et al., "Ultrasound evaluation of the radial artery in young adults - A pilot study," *Ann. Anatomy*, vol. 238, Nov. 2021, Art. no. 151763.

[35] L. Salem, J. Rey, S. P. Roddy, and R. C. Darling III, "Duplex utilization of radial artery imaging," in *Noninvasive Vascular Diagnosis*. London, U.K.: Springer, 2013, pp. 379–385.

[36] M. Sugawara, K. Niki, H. Furuhata, S. Ohnishi, and S. Suzuki, "Relationship between the pressure and diameter of the carotid artery in humans," *Heart Vessels*, vol. 15, no. 1, pp. 49–51, Jan. 2000.

[37] M. M. Budge and R. G. Gosling, "Terminology for describing the elastic behavior of arteries," *Hypertension*, vol. 41, no. 6, pp. 1180–1182, 2003.

[38] P. M. Nabeel, J. Jayaraj, K. Srinivasa, S. Mohanasankar, and M. Chenniappan, "Bi-modal arterial compliance probe for calibration-free cuffless blood pressure estimation," *IEEE Trans. Biomed. Eng.*, vol. 65, no. 11, pp. 2392–2404, Nov. 2018.

[39] J. C. Bramwell and A. V. Hill, "The velocity of pulse wave in man," *Proc. Roy. Soc. London B, Biol. Sci.*, vol. 93, no. 652, pp. 298–306, 1922.
[40] M. Grumann et al., "Sensitivity enhancement for colorimetric glucose assays on whole blood by on-chip beam-guidance," *Biomed. Microdevices*, vol. 8, no. 3, pp. 209–214, 2006.
[41] W. W. Nichols, *McDonald's Blood Flow in Arteries: Theoretical, Experimental and Clinical Principles*, 6th ed. London, U.K.: Taylor & Francis Group, 2011.
[42] Y.-L. Zheng, B. P. Yan, Y.-T. Zhang, and C. C. Y. Poon, "An armband wearable device for overnight and cuff-less blood pressure measurement," *IEEE Trans. Biomed. Eng.*, vol. 61, no. 7, pp. 2179–2186, Jul. 2014.
[43] D. Hughes, C. F. Babbs, L. Geddes, and J. Bourland, "Measurements of Young's modulus of elasticity of the canine aorta with ultrasound," *Ultrason. Imag.*, vol. 1, no. 4, pp. 356–367, 1979.
[44] J. Sola and R. Delgado-Gonzalo, *The Handbook of Cuffless Blood Pressure Monitoring the Handbook of Cuffless Blood Pressure Monitoring: A Practical Guide for Clinicians*, 1st ed. Cham, Switzerland: Springer, 2020.
[45] M. Razminia et al., "Validation of a new formula for mean arterial pressure calculation: The new formula is superior to the standard formula," *Catheterization Cardiovascular Interventions*, vol. 63, no. 4, pp. 419–425, 2004.
[46] K. L. Christensen, M. J. Mulvany, and L. T. Jespersen, "Can mean arterial pressure be estimated from measurements of systolic and diastolic blood pressure, and vice versa?" *J. Hypertension*, vol. 8, no. 4, pp. 321–326, Apr. 1990.
[47] *Noninvasivesphyg-Momanometers—Part 2–61: Clinical Investigation of Intermittent Auto-mated Measurement Type*, Int. Org. Standardization, Geneva, Switzerland, 2018.
[48] E. O'Brien et al., "European society of hypertension international protocol revision 2010 for the validation of blood pressure measuring devices in adults," *Blood Pressure Monit.*, vol. 15, no. 1, pp. 23–38, 2010.
[49] M. Nitzan, A. Romem, and R. Koppel, "Pulse oximetry: Fundamentals and technology update," *Med. Devices*, vol. 7, pp. 231–239, Jul. 2014.
[50] M. P. Bickler and L. J. Rhodes, "Accuracy of detection of carboxyhemoglobin and methemoglobin in human and bovine blood with an inexpensive, pocket-size infrared scanner," *PLoS ONE*, vol. 13, no. 3, pp. 1–12, 2018.

Cheng-Yan Guo received the B.S. degree from the National Taichung University of Education, Taichung, Taiwan, in 2014, and the M.S. degree from the National Taiwan University College of Medicine, New Taipei, Taiwan, in 2017.

He is currently the Director of Research and Development with Accurate Meditech Inc., New Taipei City, His research interests include software testing, robotics, computer vision, biosignal processing, and embedded systems.

Chi-Hung Huang is the Director of the Cardiovascular Center and Interventional Cardiovascular Department, Cathay General Hospital, New Taipei City, Taiwan.

Chia-Chi Chang received the B.S. degree from the Department of Mathematics and Information Education, National Taipei University of Education, Taipei, Taiwan, in 2015, and the M.S. degree from the National Taiwan University of Science and Technology, Taipei, in 2019.

She has been working as the Packaging Engineer at Advanced Micro Devices Inc., Hsinchu, Taiwan, since November 2019, to investigate and implement innovative technologies and evaluate ball grid array distribution rules when designing IC chips. She has specialized is in the development of machine learning algorithms for packaging design and simulation automation. Her research ranges from machine learning and automation technology to digital learning and user experience design.

Kuan-Jen Wang received the B.S. degree from Moorpark College, Moorpark, CA, USA, in 2006, and the M.S. degree from the Department of Business Management, Tatung University, New Taipei City, Taiwan, in 2021.

His research interests include raw components and product integration and production, also biosignal sensor development. His experience has product integration, production, biomedical signal sensor development of healthcare, medical devices, and technology surveys.

Tung-Li Hsieh (Member, IEEE) received the B.S. and M.S. degrees in mechanical engineering from National Cheng Kung University, Tainan, Taiwan, in 2004 and 2006, respectively, and the Ph.D. degree from the Department of Photonics and Mechanical and Electromechanical Engineering, National Sun Yat-sen University, Kaohsiung City, Taiwan, in 2012.

Now, he is an Assistant Professor with the Department of Electronic Engineering, National Kaohsiung University of Science and Technology, Kaohsiung City. His research interest includes biomedical signal sensing, signal processing, and opto-electromechanical integration. His patents include the bone conduction audio transmission device, the sound transmission device, the sound laser control lock device, the tooth vibration mode sound transmission device, and the protein battery.